

Experimental test of symmetron-field based dark energy model using neutron interferometry

Andreas Dvorak^{1,*}, Kazuma Obigane¹, Hartmut Lemmel^{1,2}, Tobias Jenke², and Stephan Sponar^{1†}

¹*Atominstytut, TU Wien, Stadionallee 2, 1020 Vienna, Austria*

²*Institut Laue Langevin, 38000 Grenoble, France*

(Dated: June 3, 2026)

We report phase shift measurements of neutron matter waves propagating in vacuum and low-pressure Argon gas, using a technique developed for neutron interferometric scattering length measurements. The experiment probes additional phase shifts induced by couplings to scalar fields. From the absence of such effects, we set stringent constraints on a scalar symmetron-field, a leading candidate for quintessence dark energy.

Introduction.—The source of dark energy, an unknown substance that manifests in the accelerated expansion rate of our Universe, is one of the most important unsolved questions in modern cosmology [1, 2]. A solution to this problem might be found in new hypothetical scalar fields with a self-interaction and a coupling to matter via a screening mechanism, accounting for dark energy [3]. The scalar field acts effectively like a cosmological constant, thereby driving the observed accelerated expansion of the Universe. The corresponding effective potential is such that a fifth force induced by the scalar field would be strongly suppressed in regions of high mass densities like on Earth. On cosmological scales, however, the ambient mass densities are very low, and the force is no longer suppressed.

There are three prominent dark energy candidates with their scalar fields described by dilaton (D) [4], symmetron (S) [5–8] and chameleon models [9]. The exponentially decreasing dilaton potential naturally arises in the strong-coupling limit of string theory [10–12] and has been proposed as a viable dark energy candidate. Initial experimental constraints have been obtained from Lunar Laser Ranging experiments [13], gravity resonance spectroscopy [14, 15], and projected constraints from Casimir-effect measurements [16], as reported in Refs. [17, 18]. In addition, Ref. [19] demonstrates that further bounds can be derived by analyzing dilaton-induced open quantum dynamics within the theoretical framework developed in Refs. [20–22]. Symmetron models, on the other hand, rely on a mechanism of spontaneous symmetry breaking analogous to that of the Standard Model Higgs field [23, 24]. Regarding the chameleon fields, we do not expect to improve the stringent limits already known (see [9] for a living review).

These models predict a quantum-mechanical phase shift for neutrons traversing a vacuum region in which the corresponding scalar field develops in the absence of matter [25–27]. The effective potentials are given by $V_{\text{eff}}(\phi, \rho) = V(\phi) + \rho A(\phi)$, where $V(\phi)$ describes the self-interactions of the field and $A(\phi)$ the coupling to the

ambient matter density ρ , with $V_{\text{D}}(\phi) = V_0 e^{-\lambda\phi/m_{\text{pl}}}$, $A_{\text{D}}(\phi) = 1 + \frac{A_2}{2} \frac{\phi^2}{m_{\text{pl}}^2}$ and $V_{\text{S}}(\phi) = -\frac{\mu^2}{2} \phi^2 + \frac{\lambda}{4} \phi^4$, $A_{\text{S}}(\phi) = 1 + \frac{\phi^2}{2M^2}$, for D and S, respectively. Here V_0 is a constant energy density, λ a dimensionless coupling parameter, A_2 a dimensionless coupling constant, m_{pl} the reduced Planck mass, and μ and M are two mass scales. The phase shift depends not only on the remaining gas pressure but also on the particular shape of the field in the region.

This paper will mainly probe the rather unexplored parameter space of symmetron models. A comprehensive analysis of the dilaton parameter space is planned for a separate paper.

Theory.—The effective potential of the scalar fields under consideration is given by

$$V_{\text{eff}}(\phi, \rho) = V(\phi) + \rho A(\phi), \quad (1)$$

where $V(\phi)$ describes the self-interactions of the field and the Weyl factor $A(\phi)$ couples to the ambient matter density ρ . The symmetron model is defined by [28]

$$V(\phi) = -\frac{\mu^2}{2} \phi^2 + \frac{\lambda}{4} \phi^4 \quad (2)$$

together with

$$A(\phi) = 1 + \frac{\phi^2}{2M^2}. \quad (3)$$

The parameters of the symmetron are the two mass scales μ and M , and the dimensionless coupling parameter λ . To neglect possible couplings to matter of higher order, we restrict our analysis to

$$\frac{\phi^2}{2M^2} < 0.1, \quad (4)$$

which leads to sharp cutoffs in the displayed exclusion plots. However, regions where neutron interferometry is sensitive and this condition does not hold have already been constrained by other experiments.

The experimental setup is such that the neutron beam is split into two paths. Along each path, the neutrons traverse a chamber containing gas. One chamber is kept at ambient pressure (Argon chamber) while the other one

* andreas.dvorak@tuwien.ac.at

† stephan.sponar@tuwien.ac.at

is evacuated (vacuum chamber). At first, the pressure difference creates a phase shift due to the well-known neutron potential of the gas. The hypothetical scalar field then creates an additional phase which can be distinguished from the gas phase by two features. First, while evacuating the vacuum chamber the gas phase fully builds up at about 10^{-2} mbar. When going to lower pressure it stays constant within the detection limit, while the scalar field phase is expected to develop only at 10^{-5} mbar or lower. Second, the scalar field phase is expected to be strongest in the chamber center and suppressed close to the chamber walls. A transverse scan of the chamber would reveal such a pattern.

To leading order, the scalar-field-induced phase shift is given by [29]

$$\varphi_D = -\frac{m_n}{k_0} \int_{\text{CFP}} U_D(\mathbf{x}) ds, \quad (5)$$

the integration extending over the classical flight path (CFP) and

$$U_D(\mathbf{x}) = \Omega_D \frac{m_n}{2M^2} (\phi^2(\mathbf{x}) - \phi_{\text{air}}^2). \quad (6)$$

Here, k_0 is the wave number of the neutron, m_n its mass, ϕ_{air} is the field value that minimizes the potential in air and Ω_X denotes the screening charge of the neutron. Computing the field of the neutron and the surrounding chamber generally constitutes a two-body problem involving the neutron and the vacuum or air-filled cavity. We approximate this problem by modeling the neutron as a classical massive sphere with a radius of 0.5 fm, consistent with QCD expectations. This approximation, referred to as Fermi screening, enables an effective treatment of neutron screening effects. Within this framework, the scalar potential is rescaled by a screening charge Ω , which ranges from 0 for a fully screened sphere to 1 for an unscreened sphere. The analytical expressions employed for the dilaton model are provided in Ref. [17].

For each field model it is necessary to compute ϕ inside the vacuum and air chamber, which amounts to solving the non-linear differential equation

$$\Delta\phi(\mathbf{x}) = V_{\text{eff},\phi}(\phi(\mathbf{x}), \rho(\mathbf{x})). \quad (7)$$

Due to the cylindrical geometry of the vacuum chamber (see Fig. 1), it follows that

$$V_{\text{eff},\phi}(\rho, \phi) = \left[\frac{1}{r} \frac{\partial}{\partial r} \left(r \frac{\partial}{\partial r} \right) + \frac{\partial^2}{\partial z^2} \right] \phi(r, z). \quad (8)$$

As a boundary condition, we require that the scalar field ϕ reaches its potential minimum ϕ_M within the shell of the vacuum and air-filled chamber, and we restrict our analysis to parameter regimes in which this assumption is justified. Owing to the absence of analytical solutions, the corresponding differential equations are solved numerically.

Experiment.—Unpolarized neutrons pass the two paths of a skew-symmetric Mach-Zehnder type interferometer, where the [220] lattice planes of silicon crystals

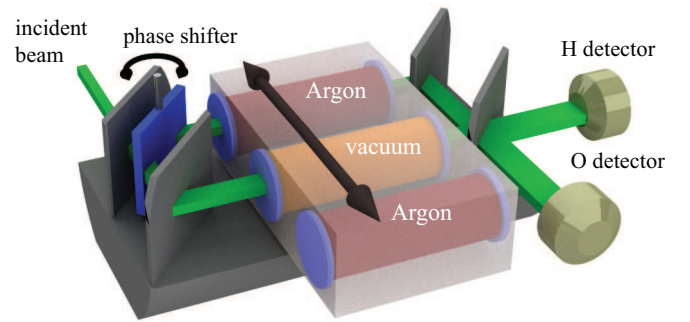


Figure 1. Schematic illustration of the neutron interferometric setup with phase shifter, air chambers, vacuum chamber, and detectors.

are used in Laue geometry (lattice planes perpendicular to the surface of the crystal plates). The interferometer has a beam separation of 50 mm over a length of 160 mm, allowing to insert individual chambers in the two beam paths, as shown in Fig. 1. A gas handling system sets a constant pressure of 1050 mbar of a pure Argon gas in the two outer chambers. The purpose of the Argon chambers is to ensure a defined gas composition and to have the same type of cell windows in both beam paths. The middle chamber is connected to a vacuum control system consisting of a pressure gauge, a motorized leak valve and two pumps. The pumps (pre-pump and turbomolecular pump) are operating continuously while a controlled amount of Argon is admitted through the leak valve to maintain a vacuum of approximately 1×10^{-6} mbar. By translating the chambers, the vacuum can be placed in the left or right beam path with one of the Argon chambers as reference in the other path. Sapphire plates on the front and the back side serve as identical windows for all three chambers. The hypothetical scalar field would induce a phase shift in addition to the Argon phase shift. This shift is probed by scanning the chamber position rel-

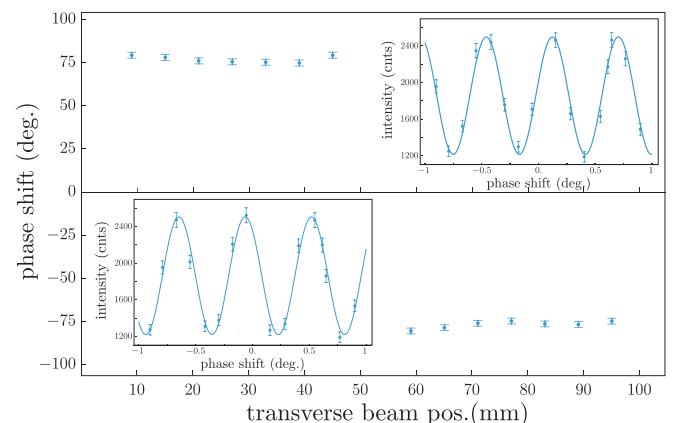


Figure 2. Intensity vs. phase shifter position at two fixed transverse beam positions (see insets) and phase shifts vs. transverse beam positions.

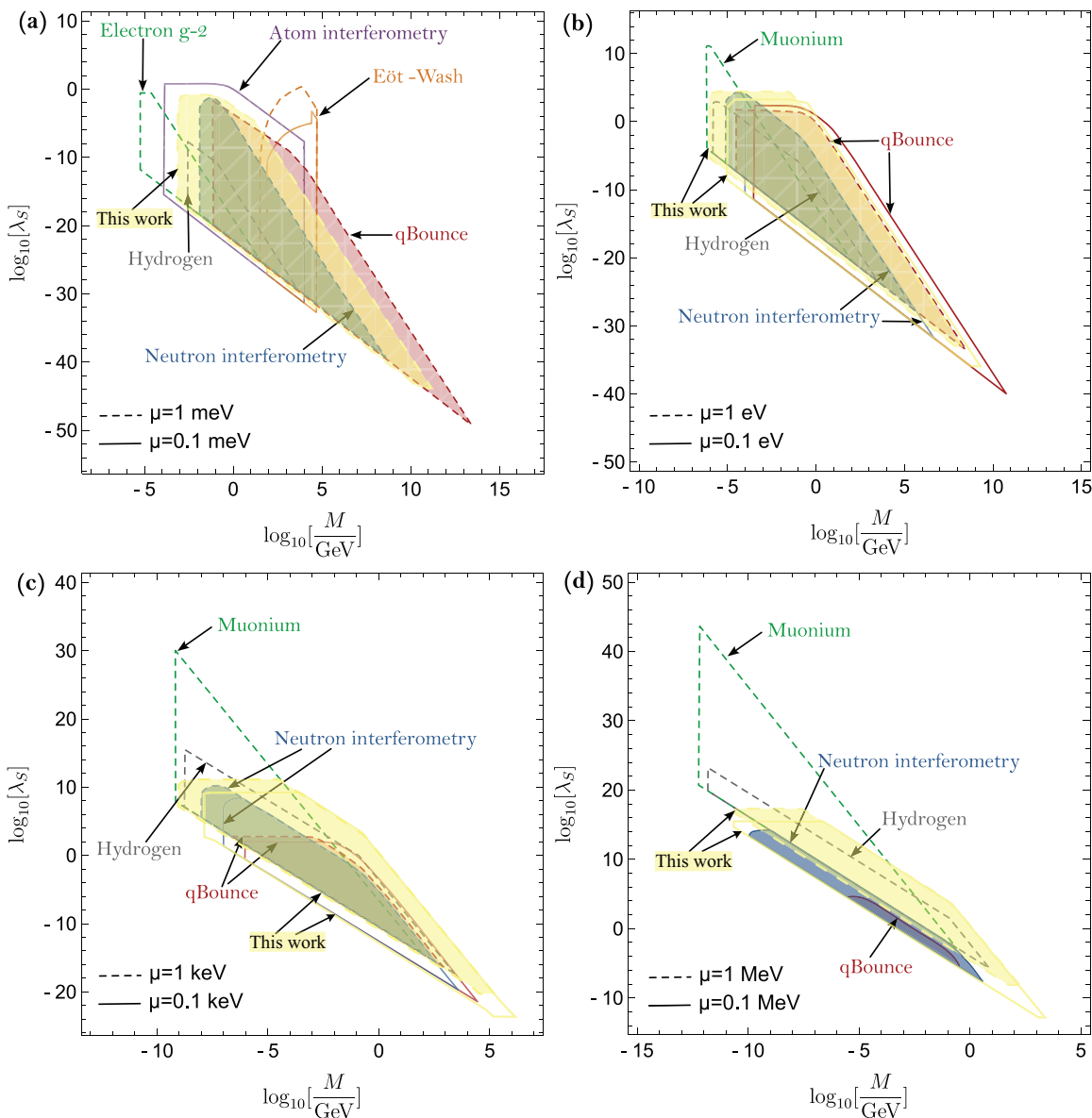


Figure 3. Exclusion plots for symmetrons at different mass scales μ , derived from Eöt-Wash [30], the atom interferometry analysis [31], investigations of hydrogen, muonium and the electron ($g-2$) [32], and analysis for qBOUNCE, neutron interferometry [33, 34].

ative to the beam (see Fig. 1), thereby probing the spatial profile of the scalar field, which is expected to be stronger at the center of the cell than near the walls.

The experiment was carried out at the neutron interferometer instrument S18 at the high-flux reactor of the Institute Laue-Langevin (ILL) in Grenoble, France. A perfect crystal silicon interferometer was operated at a Bragg angle of 45° and a monochromatic beam with mean wavelength $\lambda = 2.72 \text{ \AA}$ ($\frac{\delta\lambda}{\lambda} \approx 0.043$) and $5 \times 5 \text{ mm}^2$ beam cross section was used.

By rotating an auxiliary phase shifter (see Fig. 1) and recording the intensity oscillations between O and H detector. Such interferograms are measured before and after some parameter variation. The relative displacement of the corresponding sinusoidal curves represents the phase shift induced by the parameter change. The acquisition of each interferogram typically requires on the

order of half an hour. During this time, the intrinsic phase of the interferometer can drift due to temperature fluctuations or other environmental influences. To compensate for such drifts, the motion of the phase shifter is interlaced with the variation of the experimental parameter. Specifically, the phase shifter is rotated to a given angular position, and neutrons are counted for a certain amount of time for each parameter setting. The phase shifter is then advanced to the next position, and neutron counting is repeated for all parameter settings, and so forth. In this manner, we obtain interferograms measured simultaneously for all parameter settings. Consequently, their relative phases are free of phase drifts.

We used the largest neutron interferometer available [35] with a loop size of $50 \text{ mm} \times 160 \text{ mm}$ in order to maximize the size of the chambers. Such large single crystal interferometers are extremely sensitive to temperature

gradients, air flow, vibrations, bending, and other perturbations. Consequently, the interference contrast (fringe visibility) is limited to approximately 27 % to 45 %. The interferograms appear somewhat noisier than can be accounted for by pure counting statistics. This implies that the phase is slightly fluctuating over the duration of each interferogram acquisition. We conservatively accounted for this noise by performing a χ^2 test for each sine fit and by inflating the fit error by a factor of about 2 such that the χ^2 test was satisfied.

For each phase shifter position, we measured at seven transverse beam positions with the vacuum chamber in the left beam path and seven with the vacuum chamber in the right beam path, in order to search for bubble-like phase profiles.

Data acquisition and evaluation.—Based on the measurements acquired at 7 transverse beam positions per path (see Fig. 2, insets), a global multivariate fit was performed in which the phase was treated as the sole free parameter (see Fig. 2).

Results.—We calculated limits for λ at a fixed M and μ by comparing the calculated phase shifts ξ with the measured phase shifts $\zeta \pm \sigma$. We assume certain values

of λ and calculate the corresponding probability p ,

$$p(\lambda) = \frac{\exp\left(-\frac{1}{2}\chi(\lambda)^2\right)}{\int_0^{\lambda_{\max}} \exp\left(-\frac{1}{2}\chi(\lambda)^2\right) d\lambda}, \quad (9)$$

$$\chi(\lambda)^2 = \sum_i \frac{(\xi(\lambda)_i - \zeta_i)^2}{\sigma_i^2}. \quad (10)$$

We determined the limit λ_{lim} with 95 % confidence level by numerically solving the equation

$$\int_0^{\lambda_{\text{lim}}} p(\lambda) d\lambda = 95 \%. \quad (11)$$

The calculation is repeated for different values of M and μ yielding the following results as shown in Fig. 3. This figure shows exclusion plots of λ vs. M in GeV for different mass scales μ on a log-log scale, derived from Eöt-Wash results [30], the atom interferometry analysis [31], investigations of hydrogen, muonium and the electron ($g-2$) [32], and analysis for qBOUNCE, neutron interferometry [33, 34]. The yellow-shaded regions obtained in this work demonstrate a significant improvement over the previous qBOUNCE neutron interferometry experiment [33, 34].

Conclusions.—Using neutron interferometry, we found no evidence symmetrons but derived new limits on the coupling parameter λ for different values of M and μ .

Acknowledgments.—This research was funded in part by the Austrian Science Fund (FWF) (grant DOIs: 10.55776/P34239 and 10.55776/PAT3585625). For open access purposes, the authors have applied a CC BY public copyright license to any authors accepted manuscript version arising from this submission. The authors acknowledge the hospitality of the ILL. The data that support the findings of this study are available [36].

-
- [1] A. G. Riess *et al.* (Supernova Search Team), Observational evidence from supernovae for an accelerating universe and a cosmological constant, *Astron. J.* **116**, 1009 (1998), arXiv:astro-ph/9805201.
- [2] S. Perlmutter *et al.* (Supernova Cosmology Project), Measurements of ω and λ from 42 high redshift supernovae, *Astrophys. J.* **517**, 565 (1999), arXiv:astro-ph/9812133.
- [3] A. Joyce, B. Jain, J. Khoury, and M. Trodden, Beyond the cosmological standard model, *Phys. Rept.* **568**, 1 (2015), arXiv:1407.0059 [astro-ph.CO].
- [4] P. Brax, C. van de Bruck, A.-C. Davis, and D. Shaw, The dilaton and modified gravity, *Phys. Rev. D* **82**, 063519 (2010), arXiv:1005.3735 [astro-ph.CO].
- [5] G. Cronenberg, P. Brax, H. Filter, P. Geltenbort, T. Jenke, G. Pignol, M. Pitschmann, M. Thalhhammer, and H. Abele, Acoustic rabi oscillations between gravitational quantum states and impact on symmetron dark energy, *Nature Phys.* **14**, 1022 (2018), arXiv:1902.08775 [hep-ph].
- [6] P. Brax and M. Pitschmann, Exact solutions to nonlinear symmetron theory: One- and two-mirror systems, *Phys. Rev. D* **97**, 064015 (2018), arXiv:1712.09852 [gr-qc].
- [7] M. Pitschmann, Exact solutions to nonlinear symmetron theory: One- and two-mirror systems. ii., *Phys. Rev. D* **103**, 084013 (2021), [Erratum: *Phys.Rev.D* 106, 109902 (2022)], arXiv:2012.12752 [gr-qc].
- [8] P. Brax and S. Fichet, Quantum chameleons, *Phys. Rev. D* **99**, 104049 (2019).
- [9] C. Burrage and J. Sakstein, Tests of chameleon gravity, *Living Reviews in Relativity* **21**, 10.1007/s41114-018-0011-x (2018).
- [10] M. Gasperini, F. Piazza, and G. Veneziano, Quintessence as a runaway dilaton, *Phys. Rev. D* **65**, 023508 (2002), arXiv:gr-qc/0108016.
- [11] T. Damour, F. Piazza, and G. Veneziano, Violations of

- the equivalence principle in a dilaton-runaway scenario, *Physical Review D* **66**, 10.1103/physrevd.66.046007 (2002).
- [12] T. Damour, F. Piazza, and G. Veneziano, Runaway dilaton and equivalence principle violations, *Physical Review Letters* **89**, 10.1103/physrevlett.89.081601 (2002).
- [13] J. Müller, T. W. Murphy, U. Schreiber, P. J. Shelus, J.-M. Torre, J. G. Williams, D. H. Boggs, S. Bouquillon, A. Bourgoïn, and F. Hofmann, Lunar laser ranging: a tool for general relativity, lunar geophysics and earth science, *Journal of Geodesy* **93**, 2195 (2019).
- [14] H. Abele, T. Jenke, H. Leeb, and J. Schmiedmayer, Ramsey's method of separated oscillating fields and its application to gravitationally induced quantum phase shifts, *Phys. Rev. D* **81**, 065019 (2010).
- [15] T. Jenke, P. Geltenbort, H. Lemmel, and H. Abele, Realization of a gravity-resonance-spectroscopy technique, *Nature Phys.* **7**, 468 (2011).
- [16] R. I. P. Sedmik and M. Pitschmann, Next generation design and prospects for cannex, *Universe* **7**, 234 (2021), arXiv:2107.07645 [physics.ins-det].
- [17] P. Brax, H. Fischer, C. Käding, and M. Pitschmann, The environment dependent dilaton in the laboratory and the solar system, *Eur. Phys. J. C* **82**, 934 (2022), arXiv:2203.12512 [gr-qc].
- [18] H. Fischer, C. Käding, R. I. Sedmik, H. Abele, P. Brax, and M. Pitschmann, Search for environment-dependent dilatons, *Physics of the Dark Universe* **43**, 101419 (2024).
- [19] C. Käding, M. Pitschmann, and C. Voith, Dilaton-induced open quantum dynamics, *Eur. Phys. J. C* **83**, 767 (2023), arXiv:2306.10896 [hep-ph].
- [20] C. Burrage, C. Käding, P. Millington, and J. Minář, Open quantum dynamics induced by light scalar fields, *Phys. Rev. D* **100**, 076003 (2019).
- [21] C. Burrage, C. Käding, P. Millington, and J. Minář, Influence functionals, decoherence and conformally coupled scalars, *Journal of Physics: Conference Series* **1275**, 012041 (2019).
- [22] C. Käding and M. Pitschmann, New method for directly computing reduced density matrices, *Phys. Rev. D* **107**, 016005 (2023).
- [23] K. Hinterbichler and J. Khoury, Symmetron fields: Screening long-range forces through local symmetry restoration, *Phys. Rev. Lett.* **104**, 231301 (2010).
- [24] K. Hinterbichler, J. Khoury, A. Levy, and A. Matas, Symmetron cosmology, *Phys. Rev. D* **84**, 103521 (2011).
- [25] H. Lemmel, P. Brax, A. Ivanov, T. Jenke, G. Pignol, M. Pitschmann, T. Potocar, M. Wellenzohn, M. Zawisky, and H. Abele, Neutron interferometry constrains dark energy chameleon fields, *Physics Letters B* **743**, 310 (2015).
- [26] K. Li, M. Arif, D. G. Cory, R. Haun, B. Heacock, M. G. Huber, J. Nsofini, D. A. Pushin, P. Saggi, D. Sarenac, C. B. Shahi, V. Skavysh, W. M. Snow, and A. R. Young (The INDEX Collaboration), Neutron limit on the strongly-coupled chameleon field, *Phys. Rev. D* **93**, 062001 (2016).
- [27] H. Lemmel, M. Jentschel, H. Abele, F. Lafont, B. Guerard, C. P. Sasso, G. Mana, and E. Massa, Neutron interference from a split-crystal interferometer, *Journal of Applied Crystallography* **55**, 870 (2022).
- [28] P. Brax, C. Burrage, and A.-C. Davis, Laboratory constraints, *Int. J. Mod. Phys. D* **27**, 1848009 (2018).
- [29] D. M. Greenberger and A. W. Overhauser, Coherence effects in neutron diffraction and gravity experiments, *Rev. Mod. Phys.* **51**, 43 (1979).
- [30] A. Upadhye, Symmetron dark energy in laboratory experiments, *Phys. Rev. Lett.* **110**, 031301 (2013).
- [31] C. D. Panda, M. J. Tao, M. Ceja, J. Khoury, G. M. Tino, and H. Müller, Measuring gravitational attraction with a lattice atom interferometer, *Nature* **631**, 515 (2024).
- [32] P. Brax, A.-C. Davis, and B. Elder, Screened scalar fields in hydrogen and muonium, *Phys. Rev. D* **107**, 044008 (2023).
- [33] H. Fischer, C. Käding, H. Lemmel, S. Sponar, and M. Pitschmann, Search for dark energy with neutron interferometry, *Progress of Theoretical and Experimental Physics* **2024**, 023E02 (2024).
- [34] H. Fischer, C. Käding, and M. Pitschmann, Screened scalar fields in the laboratory and the solar system, *Universe* **10**, 10.3390/universe10070297 (2024).
- [35] M. Zawinsky, M. Baron, L. R., and H. Rauch, Testing the world's largest monolithic perfect crystal neutron interferometer, *Nuclear Instruments and Methods in Physics Research Section A* (2025).
- [36] A. Dvorak, T. Jenke, H. Lemmel, K. Obigane, and S. Sponar, Scalar field based dark energy models (2025).